VOL. 12, NO. 10, MAY 2017 ISSN 1819-6608
ARPN Journal of Engineering and Applied Sciences

www.arpnjournals.com

FLOW INDUCED VIBRATION OF A SQUARE CYLINDER WITH HIGH SCRUTON NUMBER

Mohamad Hafiz Ismail[1], Mohamed Sukri Mat Ali[1], Sheikh Ahmad Zaki Shaikh Salim[1], Masataka Shirakashi[1] and Sallehuddin Muhamad[2]
[1]Wind Engineering Laboratory, Malaysia-Japan International Institute of Technology, Universiti Teknologi Malaysia, Kuala Lumpur, Malaysia
[2]Department of Engineering, UTM Razak School of Engineering and Advanced Technology, Universiti Teknologi Malaysia, Kuala Lumpur, Malaysia

ABSTRACT

Flow over a square cylinder is numerically studied to understand the effect of reduced velocity to the transverse oscillation under the influence of high Scruton number elastic system of 4.316. For low reduced velocities, the transverse oscillation behavior can be grouped in the initial branch region. In this region, the motion is mainly controlled by the lift fluctuation. For intermediate reduced velocities, the transverse oscillation behavior is grouped in the lower branch region. In this region, its natural frequency slowly becomes significant. For high reduced velocities, the galloping region is observed. In this region, the natural frequency dominated the shape of the amplitude oscillation.

Keywords: square cylinder, elastic system, vortex induced vibration, galloping.

INTRODUCTION

This study is a part of series of investigations on the interesting features of flow over a bluff body [1, 2, 3, 4, 5, 6, and 7]. There are two main reasons why the study of flow over a bluff body is important. First, the flow structure around a bluff body is complex and there is always a new fundamental understanding is observed for every detailed investigation being carried out for this type of flow problem. Second, bluff bodies are the prominent shape for most engineering applications. However, bluff body is an efficient vortex generator [8]. It causes many flow induced problems such as high pressure drag, fluctuating forces, vibration and aerodynamic noise. Therefore, flow over a bluff body is of concern in many engineering application.

The flow over a bluff body can be controlled passively using a secondary body placed in the wake of the bluff body [9, 10]. Our previous investigations [4, 3] showed that by properly arrange a thin flat plate downstream of the bluff body, the vortex formation can be suppressed. Additionally, the plate can be designed so that the bluff body wake-plate interaction generate the same sound level as the sound emitted by the bluff body itself but out of phase. As a result, sound cancellation can be made [1].

The effect of downstream flat plate on flow induced vibration of the bluff body is still not well understood. The most related previous study is by Nakamura *et al*., [11] for the case of a rectangular cylinder with various aspect ratio (chord length over height). Even though the study focuses mainly on the galloping characteristics of the rectangular cylinder, the study elucidates clearly the effectiveness of the downstream flat plate for passive vibration control. Recently, Assi and Bearman [12] observed from their experimental investigation that when a circular cylinder is fitted with a splitter plate with 30% porosity, a lower response of transverse vibration can be obtained than a solid splitter plate.

Not a flat plate, another bluff body placed in the wake of the upstream bluff body can also affects the vibration phenomenon [13, 14, and 11]. However, the response of the vibration is governed by many parameters, such as geometry of the downstream body, gap distance between the upstream and downstream bodies and arrangement of the downstream body produce different type of vibration responses. Nevertheless, it can be concluded that the main reason for the different motion behaviors is due to the change in the formation of the large scale vortex.

Karman vortex is the prominent vortex found for any flow over bluff bodies, especially at low Reynolds number flow. The formation of this large scale vortex is originated from the free shear layer that is growing in its thickness following the entrainment of irrotational flow of the free stream into the wake [8, 4]. These make the understanding of the physic of flow for this problem warrants a systematic and proper investigation. Therefore, the current study aims on the understanding of the physics flow on the baseline case, i.e., flow over a square cylinder that is mounted on the one degree (transverse direction) elastic system.

NUMERICAL SIMULATION

Problem description

The problem geometry under investigation is a square cylinder of side length D and is allowed to move in one degree of freedom constrained by a vertical spring. The non-dimensional analysis of Khalak and Williamson [15] shows that the response of the fluctuating displacement amplitude can be written as;

$$A^* = \frac{1}{4\pi^3}\frac{C_L \sin\theta}{\left(m^* + C_A\right)\varsigma}\left(\frac{U_r}{f^*}\right)^2 f^* \quad (1)$$

where $A^* = y/D$,y is the transverse displacement, m^* is the mass ratio between the body and the displaced fluids, f^* is the amplitude frequency normalized by the natural frequency of the system, C_L is the lift coefficient, θ is the phase angle between the lift and the displacement signals and $C_A \approx 1$ is the potential added mass coefficient. Following this relationship, non-dimensional parameters are used in this study. The physical parameters of the condition are set similar to the experimental work of Kawabata *et al*. [16] and they are listed in Table-1.

Table-1. Physical parameters of the problem.

Parameter	Nomenclature	Non-dimensional	Magnitude
Reduced Velocity	U_r	$\frac{U}{f_n D}$	5-12.5
Reynolds Number	Re	$\frac{U_r D}{\nu}$	3536 - 8778
Mass ratio	m^*	$\frac{m}{\rho D^2 L}$	584.6
Damping ratio	ς	$\frac{c_{sys}}{c_{cri}}$	0.0047
Scruton number	Sc	$\frac{\pi}{2} m^* \varsigma$	4.316

This problem is represented numerically in a computational domain as shown in Figure-1. An inlet with fixed free stream reduced velocity U_r and zero pressure gradient is located 10D upstream of the cylinder, an outlet is located 20D downstream with zero velocity gradient and fixed ambient pressure. Free stream boundary condition and no slip boundary condition are set for upper and lower walls and square cylinder surfaces, respectively. The accuracy of this type of computational domain has been assessed and reported in [17].

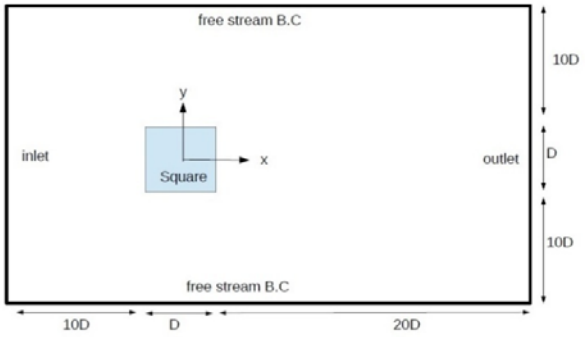

Figure-1. Sketch of the problem geometry and the computational domain (not to scale).

Flow simulation

The flow is modeled according to the conservation laws for mass and momentum in a predefined volume. This can be written in a partial different form of the governing equation (Unsteady Reynolds Averaged Navier-Stokes);

$$\rho \frac{\partial U_i}{\partial t} + \rho U_j \frac{\partial U_i}{\partial x_j} = \frac{\partial}{\partial x_j}\left[-\bar{p}\delta_{ij} + \mu\left(\frac{\partial U_i}{\partial x_j} + \frac{\partial U_j}{\partial x_i} \right) - \overline{\rho \mu_i' \mu_j'} \right] \quad (2)$$

$$\frac{\partial \rho}{\partial t} + \left(\rho U_i\right)_{,i} = 0 \quad (3)$$

where $-\overline{\rho \mu_i' \mu_j'}$ is the Reynolds stress.

Following the numerical methods of Prime *et al.* [18], who compared the result from numerical simulations and experimental measurements for the case of wake profiles of rectangular prisms, and found that the results from URANS and experiments are agree very well, the Reynols stress for the current numerical solution is solved using eddy-viscosity model based on the Boussinesq assumption;

$$-\overline{\rho \mu_i' \mu_j'} = \mu_t \left(\frac{\partial U_i}{\partial x_j} + \frac{\partial U_j}{\partial x_i} - \frac{2}{3}\frac{\partial U_k}{\partial x_k}\delta_{ij} \right) - \frac{2}{3}\rho k \delta_{ij} \quad (4)$$

where the turbulent kinetic energy (k) and the specific dissipation rate (ω) are solved using the following equations [19];

$$\frac{\partial k}{\partial t} + U_j \frac{\partial k}{\partial x_j} = P_k - \beta^* k\omega + \frac{\partial}{\partial x_i}\left[\left(\nu + \sigma_k \nu_T\right) \frac{\partial k}{\partial x_j} \right] \quad (5)$$

$$\frac{\partial \omega}{\partial t} + U_j \frac{\partial \omega}{\partial x_j} = \alpha S^2 - \beta \omega^2 + \frac{\partial}{\partial x_j}\left[\left(\nu + \sigma_\omega \nu_T\right) \frac{\partial \omega}{\partial x_j} \right] + 2\left(1 - F_1\right)\sigma_{\omega 2} \frac{1}{\omega}\frac{\partial k}{\partial x_i}\frac{\partial \omega}{\partial x_i} \quad (6)$$

where ν_T is kinematic eddy viscosity and it is defined as;

$$\nu_T = \frac{a_1 k}{\max\left(a_1 \omega, S F_2\right)} \quad (7)$$

The following closure coefficient is used in this study;

$$F_2 = \tanh\left[\left[\max\left(\frac{2\sqrt{k}}{\beta^* \omega y}, \frac{500\nu}{y^2 \omega} \right) \right]^2 \right] \quad (8)$$

where y is the distance to the next surface,

$$P_k = \min\left(\tau_{ij} \frac{\partial U_i}{\partial x_j}, 10\beta^* k\omega \right) \quad (9)$$

$$F_1 = \tanh\left\{\left\{\min\left[\max\left(\frac{\sqrt{k}}{\beta^*\omega y}, \frac{500\nu}{y^2\omega}\right), \frac{4\sigma_{\omega 2}k}{CD_{k\omega}y^2}\right]\right\}^4\right\} \quad (10)$$

$$CD_{k\omega} = \max\left(2\rho\sigma_{\omega 2}\frac{1}{\omega}\frac{\partial k}{\partial x_i}\frac{\partial \omega}{\partial x_i}, 10^{-10}\right) \quad (11)$$

$$\phi = \phi_1 F_1 + \phi_2\left(1 - F_1\right) \quad (12)$$

$$\alpha_1 = \frac{5}{9} \quad , \quad \alpha_2 = 0.44 \quad (13)$$

$$\beta_1 = \frac{3}{40} \quad , \quad \beta_2 = 0.0828 \quad , \quad \beta^* = \frac{9}{100} \quad (14)$$

$$\sigma_{k1} = 0.85 \quad , \quad \sigma_{k2} = 1 \quad , \quad \sigma_{\omega 2} = 0.856 \quad (15)$$

The 2nd-order backward scheme [20] is used for temporal discretization, the convection term is discretized using the 3rd-order QUICK scheme [21] and 2nd-order unbounded Gauss linear differencing scheme is used for the viscous term. The CFL number [22] is kept below 0.8. Computational Fluid Dynamics (CFD) solver that is based on OpenFOAM's C++ object oriented library [23] is applied to simulate this problem.

Equation of motion

The most challenging part to simulate accurately this flow-structure interaction problem is to relate the strong coupling between the flow solver and the kinematics solver. The equation of motion in a transverse direction can be written following Guilmineau and Quetey [24];

$$m\ddot{Y} + c\dot{Y} + kY = \text{Lift} \quad (16)$$

where Y is the transverse position of the cylinder surfaces, m is mass of the cylinder, c is the structural damping and k is the spring stiffness. The lift force (Lift) is assumed constant during the small time step Δt when solving this equation. To prevent any instability in the calculation, the mesh surrounding the cylinder is allowed to deform automatically based on the Laplace smoothing equation [25];

$$\nabla\cdot\left(\gamma\nabla \mathrm{u}\right) = 0 \quad (17)$$

where u is the mesh deformation velocity of the nodes in the mesh and γ is displacement diffusion, where a square of the inverse of the cell volume ($\gamma = \frac{1}{l^2}$, where l is the cell centre distance to the nearest selected boundary, i.e., square cylinder edges) has been chosen for this study. Therefore, the cell distortion is higher only when the cell distance from the cylinder surfaces is far while the cell quality near the square cylinders is preserved. Generalized Geometric-Algebraic Multi-Grid (GAMG) linear solver with Gauss Seidel smoother is used to solve iteratively Equation.(17). The tolerance for the iteration to complete is 1×10^{-9}. The mesh deformation velocity is used to update the new point positions of the mesh distributions;

$$x_{\text{new}} = x_{\text{old}} + \mathrm{u}\Delta t \quad (18)$$

After the mesh distribution has been updated, the flow equations Equation. (2) and (3) are solved.

RESULTS

For flow over a bluff body attached in the one degree flexible system, two types of flow induced vibration are expected [26]. In the low reduced velocity region, a vortex-induced vibration is observed and for the high reduced velocity, galloping is occurred. Current study for the case of a square cylinder under the influence of high Scruton number elastic system also shows the same behavior. Figure-2 shows the root mean square transverse amplitude vibration of the current study compared with the experimental measurements by Amandoles and Hemon [27] and Kawabata *et al.* [16]. A good agreement is obtained by the current numerical simulation. The current results also able to predict the regions of vortex induced vibration *(U_r < 15)* and galloping *($U_r \geq 15$)* very well when compared with the experimental measurements. Private communication with Kawabata *et al.* [16], the second peak observed by them is due to the spanwise instability that produces a rolling motion in the streamwise axis.

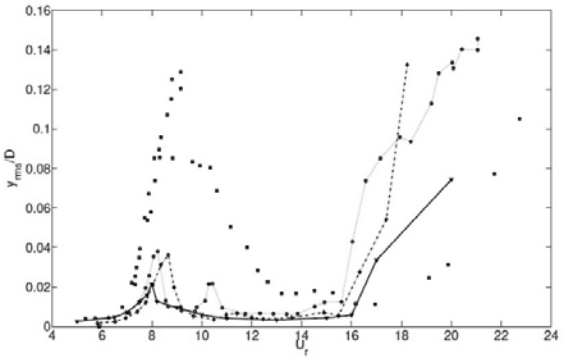

Figure-2. Root mean square transverse amplitude with reduced velocity (U^*). □ Amandoles and Hermon [27],..o.. Kawabata *et al*. [16], -◊- current (experiment),-▼-current (numerical).

Different Scruton number *(S_c)* seems not to affect the behavior of the flow induced vibration. Only the magnitude of the amplitude changes, where low S_c generates higher amplitude in the vortex-induced vibration region when compared to the high S_c elastic system. This is proven when comparing the measurement obtained by Amandoles and Hemon [27] for elastic system with S_c = 1.498 and the current numerical study with S_c = 4.316. See

Figure-2 for the comparison between the two. Slightly reduces the S_c to 3.896, and using the same equipment and procedure of Kawabata *et al.* [16], no significant different is observed. Except that the second peak has been eliminated when the signal caused by the rolling motion is carefully treated in the current study.

Power spectrum density analyses of the amplitude response for the selected cases are shown in Figure-3. The current numerical simulations predict well at the lower frequency when compared to the experimental measurements. This is expected for flow simulation using two-dimensional URANS. Doolan [28] argued that the high frequency region is mainly contributed by the spanwise instability of the flow (three-dimensional effect). However, the high frequency region is not a concern for the current study as it is not the main factor affecting the amplitude response of the flow induced vibration. This is proven by the high energy of the spectrums that are mainly distributed in the low frequency region.

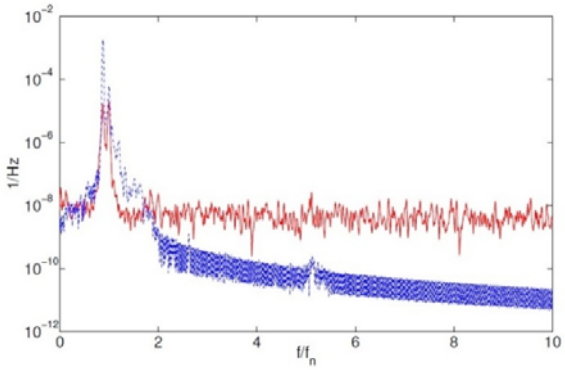

a) Ur =7

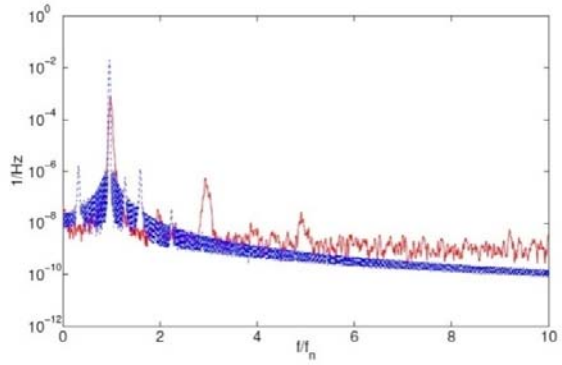

b) Ur = 8

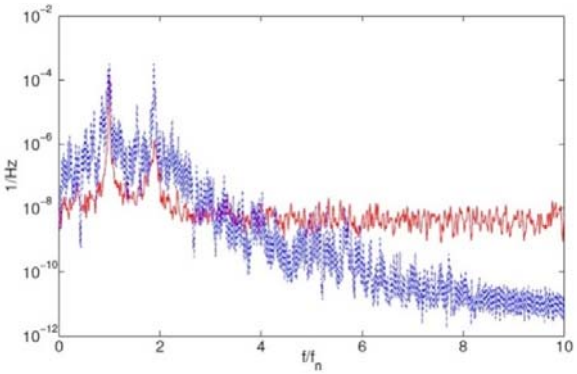

c) Ur =15

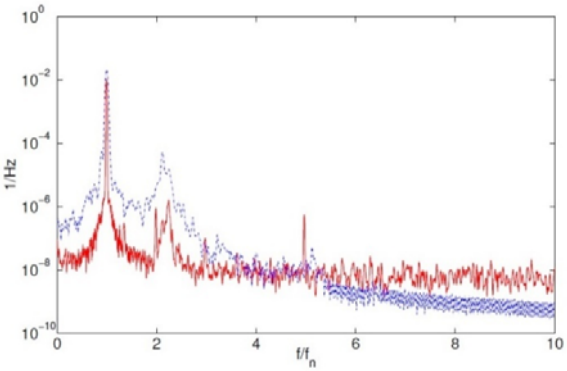

d) Ur = 17

Figure-3. Comparison of the power spectrum density for the amplitude signals between experiment (red) and numerical (blue) results.

Figure-4 shows the variation of the dominant frequencies with the reduced velocity. The amplitude frequency is almost constant that is near to the magnitude of the natural frequency, f_n. The lowest value is observed to occur at U_r = 5.5. This small drop is also observed by the experimental investigation of Amandoles and Hemon [27] for lower Scruton number (S_c = 1.498) elastic system. They argue that this is due to the existence of initial excitation branch ($U_r \leq 8.2$)and lower branch ($9 \leq U_r \leq 14$). Current study for the higher Scruton number (S_c = 4.316) also found a similar behavior. This can be observed from the lock in region ($5.5 \leq U_r \leq 8.2$) where the square cylinder oscillates transversely at the vortex shedding frequency.

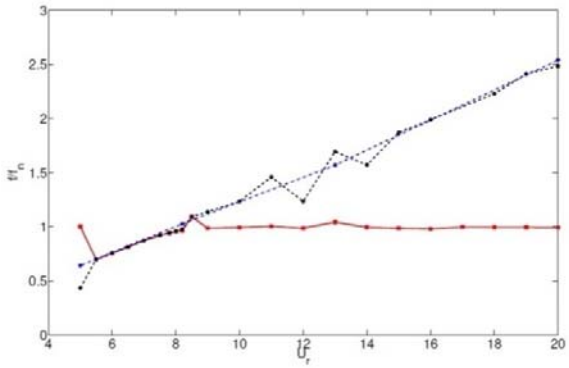

Figure-4. Frequency response of the amplitude transverse vibration (red-solid line), vortex shedding frequency of a body in transverse motion (black-broken line) and vortex shedding frequency of a body at rest (blue-dotted line).

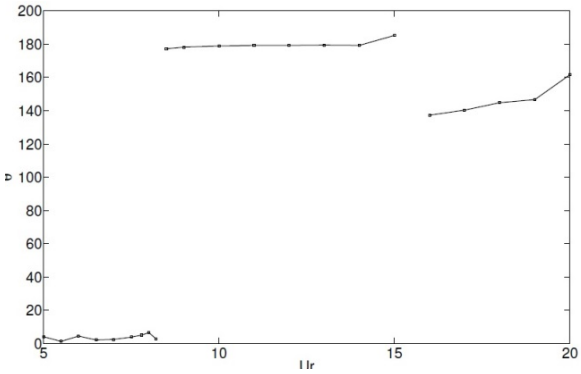

Figure-5. Phase difference between lift signal and amplitude signal. Positive sign indicates the lift signal leads the amplitude signal by θ degree.

In the initial excitation branch, the lift and amplitude oscillations are almost in phase and for the lower branch the two signals are almost out of phase. See Figure-5. Interesting feature is observed in galloping region, where the phase difference increasing with the reduced velocity. These behaviors are similar to the case of freely vibrating ($\zeta = 0$) square cylinder numerically investigated by Sen and Mittal [29] for lower Reynolds numbers flow ($60 \leq Re \leq 250$) than the current study. According to Borazjani and Sotiropoulos [30], the onset of the abrupt jump in the phase different indicates the change in the timing of the vortex shedding frequency. They also separate the initial and lower excitation branches according to this transition.

Figure-6 shows the instantaneous vorticity contours for the selected cases. The time taken is when the amplitude of the oscillation is at maximum. When the phase difference between the lift and amplitude oscillation is in phase, the shear layer on the upper surface of the square cylinder is about to grow becoming a full Karman vortex. See Figure-6 a) and b). Opposite side is observed for the out of phase condition *(U_r = 15)*. Consequently, this change in the timing of the vortex shedding make the lift attains a minima value before it increases with the reduced velocity, as argued similarly by Singh and Biswas [31]. Current study has found that the minimum lift to occur at U_r = *8.2*. This confirms again that the initial branch ends at this critical reduced velocity. For a comparison, the root mean square lift coefficient at U_r = *8* and U_r = *15* are 1.3375 and 1.4041, respectively. In the galloping region *($U_r \geq 15$)*, the shear layers from the upper and lower surfaces are found to shed at about the same time. See Figure-6(d). Thus, neither in- nor out-phase signals different is observed.

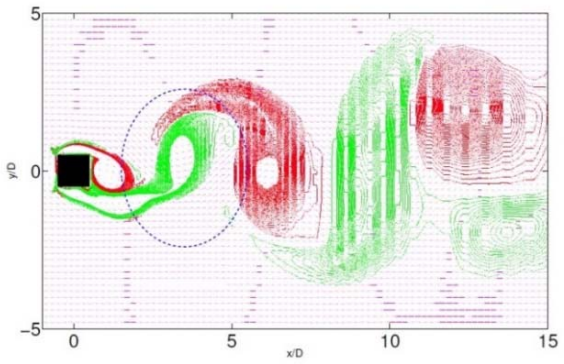

a) Ur = 7

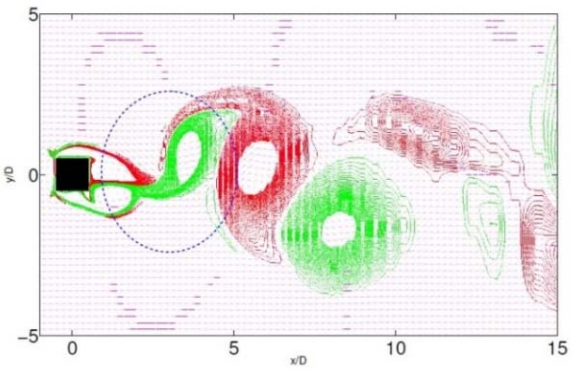

b) Ur = 8

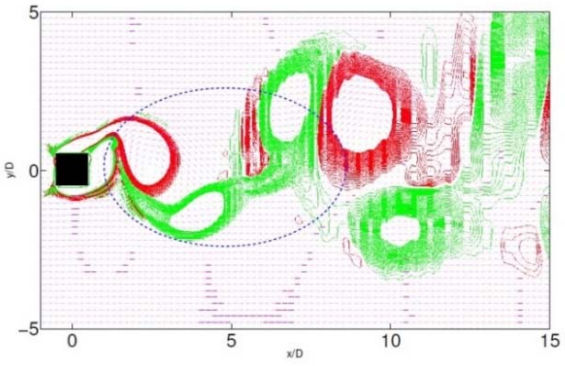

c) Ur = 15

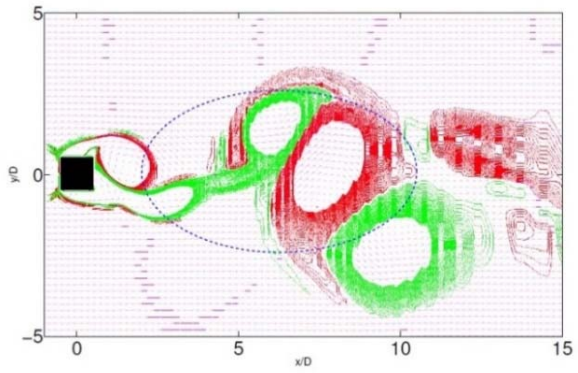

d) Ur = 17

Figure-6. Instantaneous vorticity contour when the amplitude is maximum. The contours are superimposed with instantaneous velocity vector. Broken line encircles the vortices in half cycle of amplitude oscillation.

Referring to Williamson and Roshko [32], in the lock-in region, the vortex shedding pattern can form either in 2S, 2P or P+S mode. Current study found that at each half cycle of the vibration response, a vortex shedding is formed, similar to the Karman vortex shedding. See Figures. 4 (a) and (b). Therefore, this wake pattern is in 2S mode. When the frequency ratio between the vortex shedding and amplitude oscillations $(U_r \geq 15) \frac{f_v}{f_a}$ is high, i.e. beyond the lock-in region, a vortex pair with an addition of single vortex in the other side of the wake axis is observed for each half cycle of the vibration response. This is almost similar to 2P+2S mode, but the shape is not very obvious. Referring to the map of synchronization by Williamson and Roshko [32], when $\frac{f_v}{f_a}$ is between 6 to 13, no synchronized pattern is expected, before the 2P+2S can be clearly observed when $(\frac{f_v}{f_a})$ is beyond 13.

Figure-7 shows the comparison of the fluctuating signals between the lift coefficient and the amplitude response for the selected cases. In the initial branch, the transverse motion is governed mainly by the lift force. Thus, the amplitude oscillation follows the trend of the lift force oscillation. For the lower branch, the transverse motion oscillates at the frequency near to its natural frequency. Therefore, the amplitude response not only being controlled by the lift force but mainly by its natural frequency of the system. As a result, the sinusoidal pattern of the oscillation that is initially observed in the lower branch region is not clearly seen and the synchronization between the two is loss. In the galloping region, the instability of the dynamic system itself has dominated the amplitude response and the non-synchronization between the two signals becomes obvious. Despite of that, in the lower branch ($9 \leq U_r \leq 14$) and galloping $(U_r \geq 15)$ regions, the lift forces oscillates in the same pattern, where a low and high mode pressure patterns are observed. These two modes are typical phenomenon for flow over a bluff body at high Reynolds numbers [33].

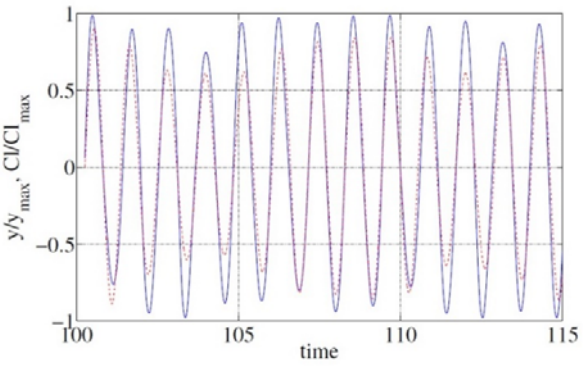

a) Ur = 8

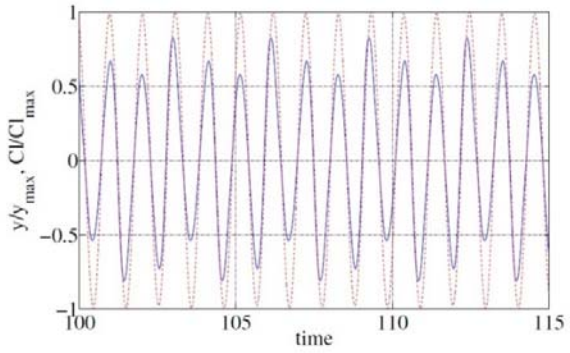

b) Ur = 8

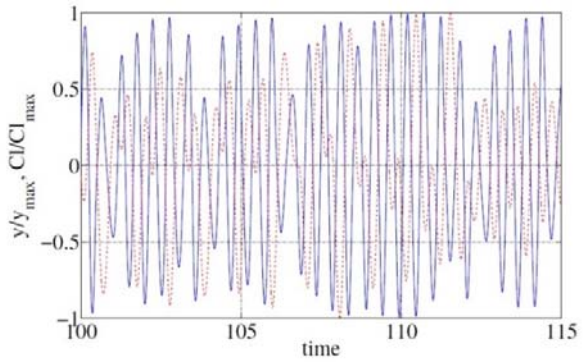

c) Ur = 15

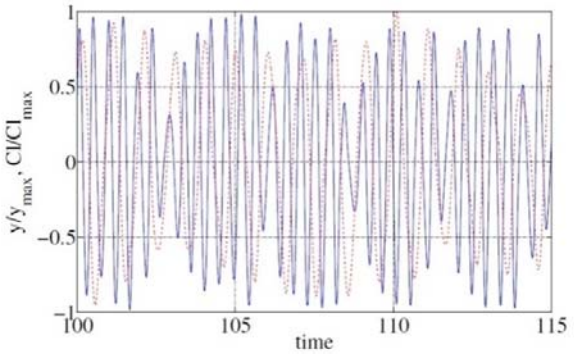

d) Ur = 17

Figure-7. Time histories of lift coefficient (C_L, solid lines), and amplitude fluctuations (y, broken lines). The values are normalized to its maximum value.

CONCLUSIONS

High Scruton number elastic system for flow over a square cylinder has been numerically investigated and compared with the experimental measurements. A good agreement between the numerical and experiments results is obtained. The amplitude response with the variation of reduced velocity is found almost similar to the low Scruton number elastic system numerically investigated by Amandoles and Hemon (Comptes Rendus Mecanique, 338 (2010) 12-17). Only that for the high Scruton number, the amplitude response is lower than the low Scruton number system. In this low amplitude response, two types of vortex shedding pattern is observed. In the initial branch region, a lock-in phenomenon is observed. In this region, two single vortices are found for every one cycle of the amplitude oscillation. This is called 2S mode. In the lower branch and galloping regions, the wake pattern is similar to 2P+2S mode, where 2 pairs of vortex shedding with one single vortex in between the two is observed. However, the pattern in not organized. This is called no synchronized mode.

ACKNOWLEDGEMENT

This research was financially supported by Malaysia Ministry of Higher Education (MOHE) under Research University Grant (RUG) project of Universiti Teknologi Malaysia (Vot No. Q.K130000.2643.09J79) and (Vot No. R.K130000.7843.4F479) also High Performance Computer (HPC) Universiti Teknologi Malaysia for the use of their supercomputer facilities. The first author also would like to acknowledge Universiti Teknologi Malaysia for the receipt of Ph.D scholarship.

REFERENCES

[1] Ali M S M, Doolan C J and Wheatley V. 2013. AIAA Journal. 51 291-301.

[2] Ali M S M, Salim S A Z S, Ismail M H, Muhamad S and Mahzan M I. 2013. Open Mechanical Engineering Journal. 7 48-57.

[3] Ali M S M, Doolan C J and Wheatley V. 2012. International Journal of Heat and Fluid Flow. 36 133-141.

[4] Ali M S M, Doolan C J and Wheatley V. 2011. Physics of Fluids (1994-present). 23 033602.

[5] Ali M S M, Doolan C J and Wheatley V. 2011. Journal of Sound and Vibration. 330 3620-3635.

[6] Ali M S M, Doolan C J and Wheatley V. 2010. Flow around a square cylinder with a detached downstream at plate at a low Reynolds number 17th Australian Fluid Mechanics Conference (Auckland, New Zealand).

[7] Ali M S M, Doolan C J and Wheatley V. 2010. Aeolian tones generated by a square cylinder with a splitter plate Proceedings of 20th International Congress on Acoustics, ICA 2010 (Sydney, Australia).

[8] Gerrard J. 1966. Journal of Fluid Mechanics. 25 401-413.

[9] Zdravkovich M. 1987. Journal of Fluids and Structures. 1 239-261.

[10] Gad-el Hak M Flow control: Passive, active and reactive flow management, 2000.

[11] Nakamura Y, Hirata K and Urabe T. 1991. Journal of fluids and structures 5 521-549.

[12] Assi G R and Bearman P W. 2014. Journal of Fluids and Structures.

[13] Assi G, Bearman P, Kitney N and Tognarelli M 2010 Journal of Fluids and Structures 26 1045-1057.

[14] Kato N, Koide M, Takahashi T and Shirakashi M. 2012. Journal of Fluids and Structures. 30 97-114.

[15] Khalak A and Williamson C. 1999. Journal of Fluids and Structures. 13 813-851

[16] Kawabata Y, Takahashi T, Haginoya T and Shirakashi M. 2013. Journal of Fluid Science and Technology. 8 348-363.

[17] Ali M S M, Doolan C J and Wheatley V. 2009. Seventh International Conference on CFD in the Minerals and Process Industries, CSIRO (CSIRO Australia, Melbourne, Australia, 2009).

[18] Prime Z, Moreau D J, Doolan C J, Ali M S M, Salleh S M and Haris S N A M. 2014. Flow modeling and noise generation of interacting prisms 20th AIAA/CEAS Aeroacoustics Conference (AIAA).

[19] Menter F R. 1994. AIAA journal. 32 1598-1605.

[20] Jasak H 1996 Error analysis and estimation for the finite volume method with applications to fluid flows Ph.D. thesis Department of Mechanical Engineering, Imperial College of Science, Technology and Medicine.

[21] Leonard B P 1979 Computer Methods in Applied Mechanics and Engineering. 19 59-98.

[22] Courant R, Friedrichs K and Lewy H. 1967. IBM J. Res. Dev. 11 215-234.

[23] Weller H G, Tabor G, Jasak H and Fureby C. 1998. Computers in physics. 12 620-631.

[24] Guilmineau E and Queutey P. 2004. Journal of Fluids and Structures 19 449-466.

[25] Jasak H and Tukovic Z. 2006. Transactions of FAMENA. 30 1-20.

[26] Sarpkaya T 2004 Journal of Fluids and Structures. 19 389-447.

[27] Amandolese X and Hemon P 2010 Comptes Rendus Mecanique. 338 12-17.

[28] Doolan C J 2010 Applied Acoustics. 71 1194-1203.

[29] Sen S and Mittal S 2011 Journal of Fluids and Structures. 27 875-884.

[30] Borazjani I and Sotiropoulos F 2009 Journal of fluid mechanics. 621 321-364.

[31] Singh S and Biswas G 2013 Journal of Fluids and Structures 41 146-155.

[32] Williamson C and Roshko A 1988 Journal of fluids and structures 2 355-381.

[33] Ohya Y 1994 Journal of fluids and structures. 8: 325-330.